remote sensing

MDPI

Article

Spatial–Temporal Variation Characteristics and Driving Factors of Net Primary Production in the Yellow River Basin over Multiple Time Scales

Ziqi Lin [1,†], Yangyang Liu [1,*,†], Zhongming Wen [1,2,*], Xu Chen [3], Peidong Han [1], Cheng Zheng [1], Hongbin Yao [1], Zijun Wang [4] and Haijing Shi [2]

[1] College of Grassland Agriculture, Northwest A&F University, Yangling, Xianyang 712100, China; 2021051664@nwafu.edu.cn (Z.L.)
[2] State Key Laboratory of Soil Erosion and Dryland Farming on Loess Plateau, Institute of Soil and Water Conservation, Northwest A&F University, Yangling, Xianyang 712100, China; shihaijingcn@nwafu.edu.cn
[3] College of Mechanical and Electronic Engineering, Northwest A&F University, Yangling, Xianyang 712100, China; chenxu@nwafu.edu.cn
[4] College of Water Resources and Architectural Engineering, Northwest A&F University, Yangling, Xianyang 712100, China
* Correspondence: 2020110044@nwafu.edu.cn (Y.L.); zmwen@ms.iswc.ac.cn (Z.W.)
† These authors contributed equally to this work.

Abstract: Vegetation net primary productivity (NPP) serves as a crucial and intuitive indicator for assessing ecosystem health. However, the nonlinear dynamics and influencing factors operating at various time scales are not yet fully understood. Here, the ensemble empirical mode decomposition (EEMD) method was used to analyze the spatiotemporal patterns of NPP and its association with hydrothermal factors and anthropogenic activities across different temporal scales for the Yellow River Basin (YRB) from 2000 to 2020. The results indicate that: (1) the annual average NPP was 236.37 g C/m^2 in the YRB and increased at rates of 4.64 g C/m^2/a^1 ($R^2 = 0.86$, $p < 0.01$) during 2000 to 2020. Spatially, nonlinear analysis indicates that 72.77% of the study area exhibits a predominantly increasing trend in NPP, while 25.17% exhibits a reversing trend. (2) On a 3-year time scale, warming has resulted in an increase in NPP in the majority of areas of the study area (69.49%). As the time scale widens, the response of vegetation to climate change becomes more prominent; especially under the long-term trend, the percentage areas of the correlation between vegetation and precipitation and temperature increased with significance, reaching 48.21% and 11.57%, respectively. (3) Through comprehensive time analysis and multivariate regression analysis, it was confirmed that both human activities and climate factors had comparable impacts on vegetation growth. Among different vegetation types, climate was still the main factor affecting grassland NPP, and only 15.74% of grassland was affected by human activities. For shrubland, forest, and farmland, human activity was a dominating factor for vegetation NPP change. There are still few studies on vegetation change using nonlinear methods in the Yellow River Basin, and most studies have not considered the effect of time scale on vegetation evolution. The findings highlight the significance of multi-time scale analysis in understanding the vegetation dynamics and providing scientific guidance for future vegetation restoration and conservation efforts.

Keywords: net primary productivity; climate change; human activities; Yellow River Basin; multiple time scale analysis

check for updates

Citation: Lin, Z.; Liu, Y.; Wen, Z.; Chen, X.; Han, P.; Zheng, C.; Yao, H.; Wang, Z.; Shi, H. Spatial–Temporal Variation Characteristics and Driving Factors of Net Primary Production in the Yellow River Basin over Multiple Time Scales. *Remote Sens.* **2023**, *15*, 5273. https://doi.org/10.3390/rs15225273

Academic Editor: Jochem Verrelst

Received: 3 August 2023
Revised: 4 October 2023
Accepted: 14 October 2023
Published: 7 November 2023

Copyright: © 2023 by the authors. Licensee MDPI, Basel, Switzerland. This article is an open access article distributed under the terms and conditions of the Creative Commons Attribution (CC BY) license (https://creativecommons.org/licenses/by/4.0/).

1. Introduction

The Intergovernmental Panel on Climate Change's (IPCC) sixth assessment report showed that global warming has accelerated in the last 40 years, resulting in serious impacts on ecosystems [1]. Vegetation is a guiding hand on terrestrial ecosystems and was

considered as highly responsive to climate factors and human activities [2–4]. Monitoring vegetation dynamics and understanding the drivers of its change become key issues in global change [5]. Net primary productivity (NPP) refers to the net accumulation of organic matter produced by green plants through photosynthesis over a given time and area [6–8], which is a crucial parameter for assessing vegetation dynamics and remains a pivotal part in the terrestrial carbon cycle [9]. Increasing NPP reflects ecosystem recovery, while decreasing NPP indicates ecosystem degradation [10]. Previous studies have shown that vegetation NPP is under strong threat from both intense climate change and anthropogenic activities [11,12]. Climate change (especially temperature and precipitation) has a great effect on vegetation [4]. With accelerated urbanization and the increasing global population, the influences on vegetation changes were enhanced by anthropogenic activities such as urban construction, cultivation, ecological management, and restoration [13–15]. Thus, understanding the spatial and temporal patterns of NPP and its interactions with environmental factors (i.e., climate factors and anthropogenic factors) has been the focus of global change studies during the past several decades.

In recent years, many researchers have shown that the long-term changes of vegetation and climate are mostly nonlinear and complex processes with inconsistent time scales [7]. The linear regression model and single time scale have certain limitations [16–18]. On the one hand, single time scale is inadequate for accurately capturing the comprehensive microscopic features of vegetation change and their spatial–temporal patterns, which may underestimate the influence of climate on vegetation variation [19]. The rate of vegetation growth is not constant [20]. Some important information on various time scales may be overlooked, such as the growth characteristics of vegetation in short and long periods [21,22]. On the other hand, under the linear and stationary assumptions, hidden information regarding the correlation of climate changes and NPP may be overlooked, leading to an enlargement of uncertainty in the relationship [14]. Therefore, it is crucial to employ appropriate methodologies for comprehending the relationship between climate change and human activities on NPP dynamics in multiple time scales under the nonlinear hypothesis.

Ensemble empirical mode decomposition (EEMD) is widely used for time–frequency analysis, which is suitable for nonlinear time series [23]. It can decompose them into several intrinsic mode function (IMF) components and a residual [24]. The residuals may exhibit monotonicity or feature a single extreme value, which shows a long-term trend [7]. Recently, some studies have begun to use EEMD in ecological research. Liu et al. [12] found that EEMD detrend analysis was superior to linear detrend analysis in assessing the relationship between climate change and vegetation NPP. Xu et al. [25] used integrated empirical mode decomposition (EEMD) to study the time-varying trends of vegetation along the Silk Road Economic Belt during 1981–2016 and its possible responses to various driving factors. This research has confirmed the applicability of EEMD in nonlinear analysis of vegetation dynamics and demonstrated that IMFs can effectively reflect the dynamics of vegetation change across various temporal scales [12,18,25–28].

The Yellow River Basin (YRB) is a crucial ecological restoration region in China, playing an indispensable role in ecological environment, production, food security, and other fields [29–31]. Following the implementation of the Grain for Green Program (GGP), the process of vegetation greening in the Yellow River Basin has been accelerated [32]. However, the vegetation is highly sensitive to climate, with fragile ecological conditions in YRB, which faced serious environmental issues such as soil erosion and grassland degradation [33,34]. Over the last several decades, there has been a noticeable change in the YRB due to pressing ecological issues and the execution of vegetation rehabilitation policies [35]. Current evidence suggests that climate changes are the main controlling factors of NPP changes, particularly temperature and precipitation [36–39]. In the YRB, vegetation NPP exhibited a significant negative correlation with temperature in the majority of the central region of the YRB [32], and precipitation was the dominant component influencing grassland NPP in the source area of the YRB [40].

2. Materials and Methods

2.1. Study Area

The Yellow River ranks as the second longest river in China, spanning a whole length of 5464 km [40]. It has its origins in the Bayan Har Mountains of the Qinghai–Tibet Plateau. It passes through the Inner Mongolia Plateau, the Loess Plateau, and the Yellow Huai-hai Plain from west to east [28]. The location of the YRB (32°10′–41°50′N,95°53′–119°05′E) is situated in central and northern China, covering about 795,000 km^2 [41]. It is attached to nine provincial administrative regions (including Qinghai, Sichuan, Gansu, Ningxia, Inner Mongolia, Shaanxi, Shanxi, Henan, and Shandong). The YRB has a complex and diverse terrain. It passes through the three ladders of the topography in China. The elevation ranges from −9 to 6217 m and the western region exhibits high values while the eastern region shows low (Figure 1). Due to its unique geographical location, the YRB plays a pivotal role in vegetation restoration projects in China. Over the last two decades, China's government has carried out series of ecological restoration initiatives aimed at improving environmental degradation and promoting high-quality development in the area [11,42].

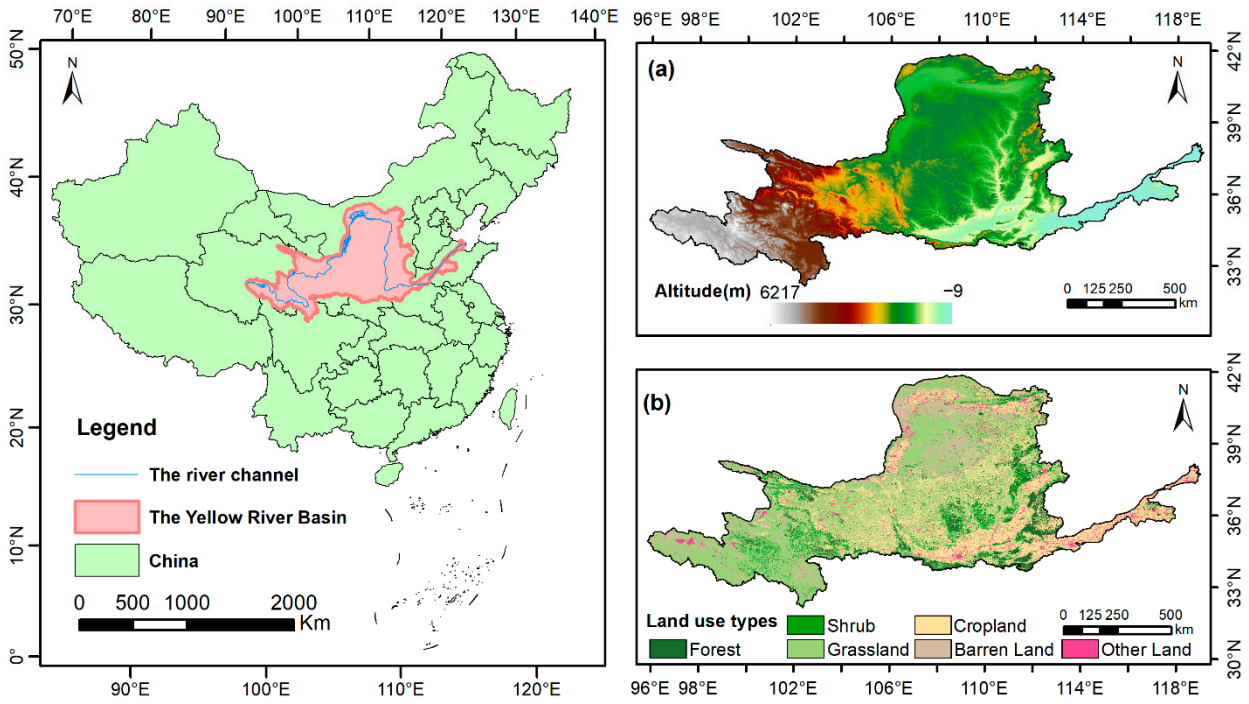


Figure 1. Study area: (**a**) elevation; (**b**) land cover types in the YRB.

The Yellow River Basin is a typical arid and semi-arid climate. The spatial distribution exhibits a significant disparity of climate, and both precipitation and temperature show a declining trend from southern to northern regions, as well as eastern to western areas. The annual precipitation of the basin ranges from 700 to 1800 mm, and the annual average temperature reaches up to 7 °C; the characteristics of temperature and precipitation during 2000 to 2020 are shown in Figure S3a,b,e,f. There are various land-use resources in the region. Grassland, cropland, and forest are the primary land-use types, which account for approximately 69.91%, 19.97%, and 4.55% of the whole spatial region in the YRB (Figure 1).

2.2. Data Source and Preprocessing

The data used in this study are shown in Table 1.

Table 1. Date type and source.

Variables	Period	Original Spatial Resolution	Dataset	Data Source
NPP	2000–2020	Yearly/500 m	MOD17A3HGF	https://developers.google.com/earth-engine/datasets/catalog/MODIS_061_MOD17A3HGF (accessed on 6 January 2023)
DEM	2018	30 m		https://www.gscloud.cn/ (accessed on 6 May 2023)
Temperature	2000–2020	Monthly/1 km	China 1 km resolution monthly average temperature dataset	http://loess.geodata.cn (accessed on 18 January 2023)
Precipitation	2000–2020	Monthly/1 km	China 1 km resolution monthly average precipitation dataset	http://loess.geodata.cn (accessed on 18 January 2023)
Population density	2000–2020	1 km	Gridded Population density of the World (GPW), Version 4	https://cds.climate.copernicus.eu/ (accessed on 6 January 2023)
Night-time light	2000–2020	500 m		https://doi.org/10.1038/s41597-020-0510-y (accessed on 6 January 2023)
Land-use type	2015	1 km	Land-use dataset in China (1980–2015)	http://www.resdc.cn/ (accessed on 6 January 2023)

2.2.1. Net Primary Productivity Data

The NPP time series data spanning from 2000 to 2020 were obtained from MOD17A3HGF, with a 500 m spatial resolution and an 8d temporal resolution, which were obtained through Google Earth Engine (GEE, https://code.earthengine.google.com/ accessed on 6 January 2023). The data format is GeoTIFF and the geographical coordinate projection system is WGS-84. We directly obtained these MODIS products in the YRB and avoided complicated pre-processing steps including mosaic, reprojecting, and extracting [43]. The MODIS NPP is defined as the difference between GPP and respiration, including maintenance and growth components. The dataset is based on the BIOME-BGC model and the LUE model, which simulate the daily biochemical cycles of vegetation and soil in terrestrial ecosystems. MODIS NPP products have been validated and are consistent with estimates of eddy correlated flux tower communities [44,45]. The dataset has been widely used in environmental monitoring, global ecosystem carbon cycle, and vegetation growth variation [46,47]. The MODIS NPP estimation method is as follows [45]:

$$NPP = GPP - R_m - R_g \quad (1)$$

where R_m is annual plant maintenance respiration; R_g is the energy cost for constructing organic compounds fixed by photosynthesis.

2.2.2. Digital Elevation Model

Digital elevation model (DEM) data were acquired from the geospatial data cloud (https://www.gscloud.cn/, accessed on 6 January 2023), with a spatial resolution of 30 m. We utilized ArcGIS 10.8 to process the DEM data and extracted it from the vector boundary of the YRB.

2.2.3. Meteorological Data

The monthly total precipitation and monthly mean temperature data were acquired from the Loess Plateau Scientific Data Center (http://loess.geodata.cn, accessed on 18 January 2023), which come from 722 standard meteorological stations in China (Figure S1). To ensure the accuracy of calculated data matching, we used ANUSPLIN software (Vrsn 4.3) to interpolate at a spatial resolution of 1 km.

2.2.4. Human Activity Factors

The analysis of anthropogenic activity across the study area is based on the population density, night-time light, and land-use type. Long-time-series population density dataset was acquired from the World Population Density Map published by World Pop (https://hub.worldpop.org, accessed on 6 January 2023, Gridded Population density of

the World, Version 4) (Figure S3d,h). The night-time light (NTL) datasets were obtained from the research of a harmonized global night-time light dataset 1992–2018 by Li et al. [5], which is the most integrated and reliable long-time-series dataset available. This dataset was collected coordinating the mutually calibrated NTL observations in the Defense Meteorological Program (DMSP) data with the simulated DMSP-like NTL observations from the Visible Infrared Imaging Radiometer Suite (VIIRS) data (Figure S3c,g).

2.2.5. Land-Use Data

Land-use type data were adopted from the products of the Chinese Academy of Sciences Resource and Environmental Science Data Center (http://www.resdc.cn/, accessed on 6 January 2023) with a spatial resolution of 1 km. The data were classified into 6 ground feature categories: grassland, forest, cropland, shrubland, waterbody, construction land, and bare land. This study focuses on the spatiotemporal characteristics and driving factors of NPP in the Yellow River Basin during the past 20 years. Therefore, we assumed that the vegetation types remained unchanged during 2000 to 2020, and the analysis was based on the vegetation types in 2015.

2.3. Methods of Analysis

2.3.1. Theil–Sen Median Trend Analysis and Mann–Kendall Test

The Theil–Sen median trend analysis is widely used in various fields due to its robustness and simplicity. The method can effectively avoid the interference of missing data and outliers to the time series [48], and the formula for calculation is outlined as follows.

$$\beta = Median\left(\frac{\mathrm{NPP}_i - \mathrm{NPP}_j}{i-j}\right) \quad (2)$$

where i and j are the numbers of years ($1 < j < i < \mathrm{n}$); NPP_i and NPP_j are the sample time series data sets; Median is the median function. β is the estimated median slope. When $\beta > 0$, NPP has an increasing trend; when $\beta < 0$, NPP has a decreasing trend.

The Mann–Kendall (MK) test [49,50] is insensitive to measurement error and can effectively reject outliers, and is widely used to test the significance of data trends in long-term time series [37]. The calculation formula is as follows:

$$S = \sum_{i=1}^{n-1} \sum_{j=i+1}^{n} sgn\left(\mathrm{NPP}_j - \mathrm{NPP}_i\right) \quad (3)$$

$$sgn\left(\mathrm{NPP}_j - \mathrm{NPP}_i\right) = \begin{cases} 1, \mathrm{NPP}_j - \mathrm{NPP}_i > 0 \\ 0, \mathrm{NPP}_j - \mathrm{NPP}_i = 0 \\ -1, \mathrm{NPP}_j - \mathrm{NPP}_i < 0 \end{cases} \quad (4)$$

where n is the number of dataset in the sequence; S is the test statistic; $sgn()$ is the symbolic function.

The standard normal test statistic Z was used for the significance test. In the confidence level of 95% (significance level, alpha = 0.05), $|Z| \geq 1.96$ and in the confidence level of 99% (significance level, alpha = 0.01), $|Z| \geq 2.58$. The trend is classified into five categories: extremely significant increase (ESI), significant increase (SI), insignificant change (IN), significant decrease (SD), and extremely significant decrease (ESD).

$$Z = \begin{cases} \frac{S-1}{\sqrt{VAR(S)}}, S > 0 \\ 0, S = 0 \\ \frac{S+1}{\sqrt{VAR(S)}}, S < 0 \end{cases} \quad (5)$$

VAR represents variance derived from the Mann–Kendall Test, and the expression for the VAR is as follows:

$$VAR(S) = \frac{n(n-1)(2n+5)}{18} \quad (6)$$

where n is the number of the time series ($n > 10$).

2.3.2. Ensemble Empirical Mode Decomposition (EEMD) Method

In this study, ensemble empirical mode decomposition (EEMD) was employed to analyze the spatiotemporal characteristics of vegetation NPP and climate variability at pixel scale over the multiple time scales. As a common method for processing in time-frequency domain, empirical mode decomposition (EMD) can overcome the problem of non-adaptive basis function in wavelet processing [14]. Using the EMD method, the original data sequence x(t) is decomposed into n components (intrinsic mode functions, IMFi, i = 1, 2, . . ., n) and a residual. However, EMD suffers from signal mixing problem in different modes. To solve this problem, Wu and Huang [32] designed a new noise-assisted signal analysis method to improve and optimize the signal processing performance of EMD, called EEMD. The decomposition steps are as follows:

Superimpose a random Gaussian white noise sequence $\omega_i(t)$ to the original signal x(t). Set 0.2 times standard deviation of the original signal to the amplitude of the Gaussian white noise sequences.

$$x_j(t) = x(t) + \omega_j(t),\ j = 1, 2, \ldots np \tag{7}$$

where np is a number of Gaussian white noise sequence, which was adopted as 1000 in this study.

Decompose the new signal x(t) using EMD.

$$x(t) = \sum_{i=1}^{n} imf_i(t) + R_n(t) \tag{8}$$

where $imf_i(t)$ and R_n (t) denote the IMF and residue from x(t) with EMD method. IMF (imf_i, i = 1, 2, . . ., n, where n is the length of time).

The IMF components on EMD and residuals are averaged to obtain the ith IMF $imf_n(t)$ and r_n on EEMD, as follows:

$$imf_i(t) = \frac{1}{np} \sum_{j=1}^{np} \mathrm{IMF}_{ij}(t) \tag{9}$$

$$r_n = \frac{1}{np} \sum_{j=1}^{np} r_{nj}(t) \tag{10}$$

Furthermore, the mean period of IMF_i component can be calculated by counting the value of local maxima and then dividing that number by time length (n). To determine the relative relevance of each IMF component and the residual, the variance contributions were calculated as follows:

$$V_{imf} = \frac{Vr(imf_i)}{\left[\sum_{i=1}^{n} Vr(imf_i) + Vr(r_n)\right]} \tag{11}$$

$$V_r = \frac{Vr(r_n)}{\left[\sum_{i=1}^{n} Vr(imf_i) + Vr(r_n)\right]} \tag{12}$$

where V_{imf} and V_r stand for the variance contributions of the IMF_i component and residue (r_n), respectively. V_r (imf_i) and $V_r(r_n)$ are the variance of the IMF_i component and residue (r_n).

Based on EEMD detection, the variation in NPP trend was divided into five categories: monotonically increasing trends (MI), monotonically decreasing trends (MD), initially increasing then decreasing (ID), initially decreasing then increasing (DI), and nonsignificant changes (IN).

2.3.3. Correlation Analysis Method

In this study, the relationship between vegetation NPP and meteorological factors (temperature and precipitation) were analyzed by the pixel-based Pearson correlation coefficient [18]. The equations are as follows.

$$R = \frac{\sum_{i=1}^{n}(x_i-\overline{x})(y_i-\overline{y})}{\sqrt{\sum_{i=1}^{n}(x_i-\overline{x})^2\sum_{i=1}^{n}(y_i-\overline{y})^2}} \quad (13)$$

where R is the correlation coefficient of x and y; x_i and y_i are the values of x and y in year i; $\overline{x}$ and $\overline{y}$ are the means of x and y; and n is the number of years. In order to judge the correlation more clearly between vegetation NPP and climate factors in the study area, we set the threshold for the Pearson's R at ± 0.4 in order to analyze vegetation dynamics more effectively by excluding data points with R values less than -0.4 or greater than 0.4.

2.3.4. Multivariate Regression Analysis (MLR)

In this study, climate variables were used as explanatory variables, and a stepwise MLR model was developed with NPP. At present, this method has been widely applied in the field of vegetation ecology [51,52]. With the standardized MLR model, the relative contribution of an independent variable can be calculated by the following formula:

$$Y = a_1'X_1 + a_2'X_2 + \cdots + a_n'X_n \quad (14)$$

where Y is the NPP, X_i is the variable (i.e., the precipitation, temperature, population density, and night-time light), a_i $(1 < i < n)$ represents the standard partial regression coefficient of i variable for MLR.

Furthermore, the relative contribution of the independent variables can be defined as [53,54]:

$$\mu_i = \frac{|a_i|}{\sum_{i=1}^{n}|a_i|} \quad (15)$$

The μ_i is the relative contribution.

3. Results

3.1. Data Validation

MODIS data have been proven accurate in production, and many studies have used such products to carry out many studies in the YRB/Loess Plateau [55–57], which proves the reliability of MOD17A3 products in this basin. At present, there are generally two ways to verify the net primary productivity data simulated by a model: one is to compare it with actual data, and the other is to compare it with other model estimates. Due to the limited sampling amount of measured data, the representative regions are often difficult to match spatially with the net primary productivity model simulation data based on remote sensing. Problems caused by scale effect make it difficult to verify net primary productivity simulation data.

In order to further verify the accuracy of MOD17 NPP products in the YRB, we selected Chen's data on the annual net primary productivity of terrestrial ecosystems in China from 2000 to 2015, and masked the data as the research area of this study [58]. Specifically, Chen et al. used China's monthly land meteorological data from 1985 to 2005, national soil texture data, and land cover and vegetation index data products based on MODIS and AVHRR remote sensing images to drive the Carnegie–Ames–Stanford approach (CASA) model to estimate the NPP data. A 1-km grid dataset of monthly net primary productivity of terrestrial ecosystems north of 18°N in China during 1985–2005 was developed. The data development range is 18°N–53.5°N, 65°E–138°E, in which the land and sea parts outside China are set to zero, and the rest of the data are NPP values. The data is stored in .tif format with a resolution of 1 km (https://www.geodoi.ac.cn/edoi.aspx?DOI=10.3974/geodb.2019.03.02.V1, accessed on 6 January 2023). The locations of sampling points are shown in Figure 2. The relationship diagram between sampling points and MOD17A3 NPP

values in the YRB and Chen's data was added (Figure 3). The fishing net map was created to sample the mean values of NPP simulated by Chen using the CASA model and NPP MOD17A3 from 2000 to 2015 (R^2 = 0.60). The correlation analysis of the two sets of data shows that the MOD17A3 NPP data have a good linear relationship with the NPP simulated by Chen. Meanwhile, we also collected the NPP data from a previous study to further verify the accuracy of MOD17 NPP in the study area [40,41]. The specific NPP comparison results can be seen in Figure S2. Overall, the results show that the MOD17A3 NPP is consistent with the BIOME-BGC NPP and LUE NPP, with a statistical relationship of R^2 = 0.84 and 0.66, respectively, implying that the MOD17A3 NPP data can be well applied to NPP research in the study area.

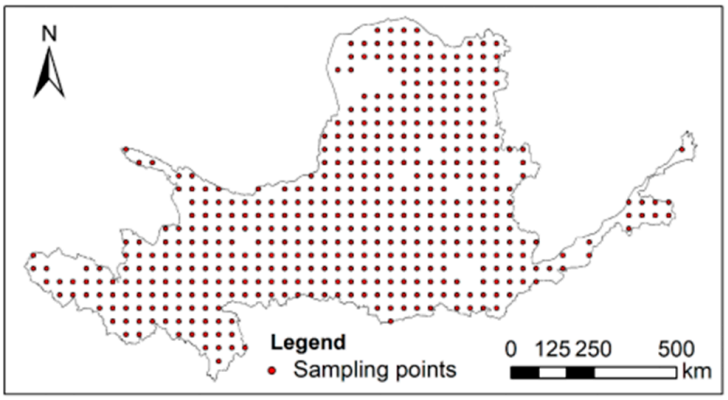


Figure 2. Sampling points for NPP in the Yellow River Basin.

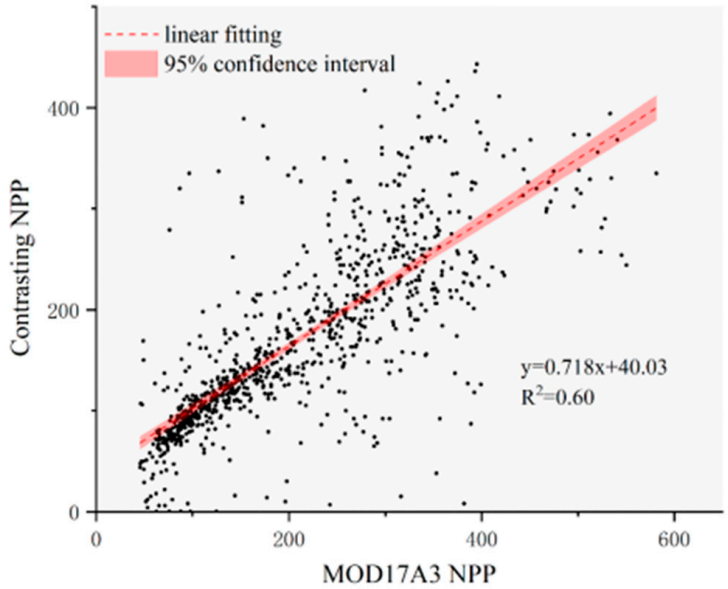


Figure 3. Relationship between MOD17A3 NPP and CASA NPP estimation.

3.2. Spatiotemporal Variation of NPP in the YRB

3.2.1. Temporal Variation of NPP

As shown in Figure 4, the mean annual NPP was 236.37 g C/m^2 in the YRB from 2000 to 2020. The average annual NPP increased significantly from 175.23 g C/m^2 in 2000 to 273.28 g C/m^2 in 2020 at rates of 4.64 g C/m^2/a^1 (R^2 = 0.86, $p < 0.01$). The annual average NPP values range from 171.74 to 289.32 g C/m^2, with the lowest value in 2001 and the highest in 2018. In terms of vegetation types, the average NPP values for different vegetation types rank in descending order as follows (g C/m^2): forest (503.73) > cropland (384.53) > grassland (243.95) > shrubland (209.12). The interannual variation trend of NPP

across different vegetation types exhibits an upward trend, which is consistent with the YRB. The largest increase (202.67 g C/m^2, $p < 0.01$) in NPP was found in forest, while the smallest was observed in shrubland (90.05 g C/m^2, $p < 0.01$).

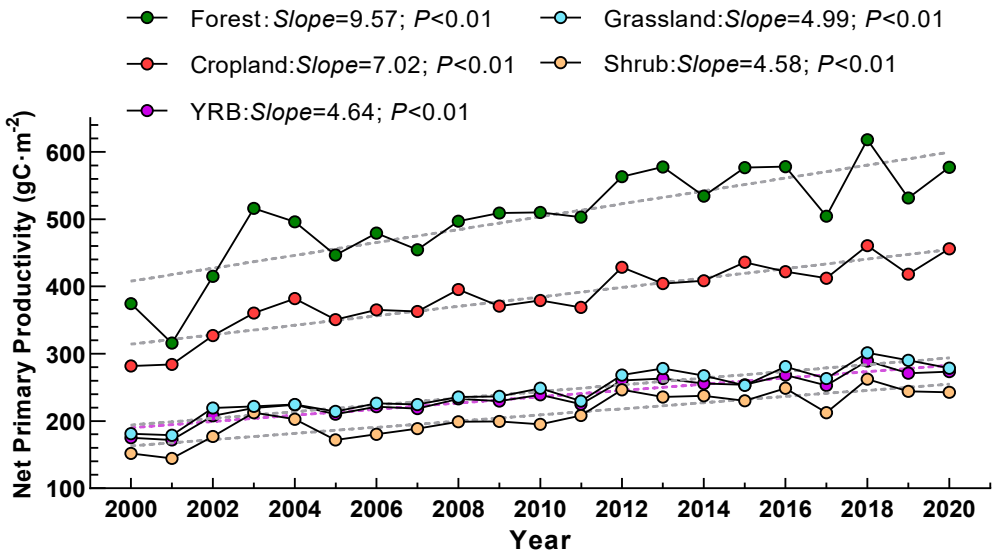


Figure 4. The interannual variation of the annual average NPP.

3.2.2. Spatial Pattens of NPP

Spatially, the vegetation NPP shows a strong spatial heterogeneity. The mean NPP ranges from 12.48 g C/m^2 to 1011.38 g C/m^2 during 2000–2020 in the YRB (Figure 5d). The regions with higher NPP values were mostly observed in the southeast of the YRB, and the lower NPP values could be detected in the northwest of the Loess Plateau and the source area of the Yellow River. Statistically, the percentage of high-value regions (NPP > 400 g C/m^2) were estimated to have increased from 4.93% in 2000 to 33.5% in 2020 (Figure 5a,b). The areas with an upward trend in NPP values constituted over 97% of all pixels. In contrast, the areas experiencing a declining trend in NPP only accounted for 2.92% (Figure 5c).

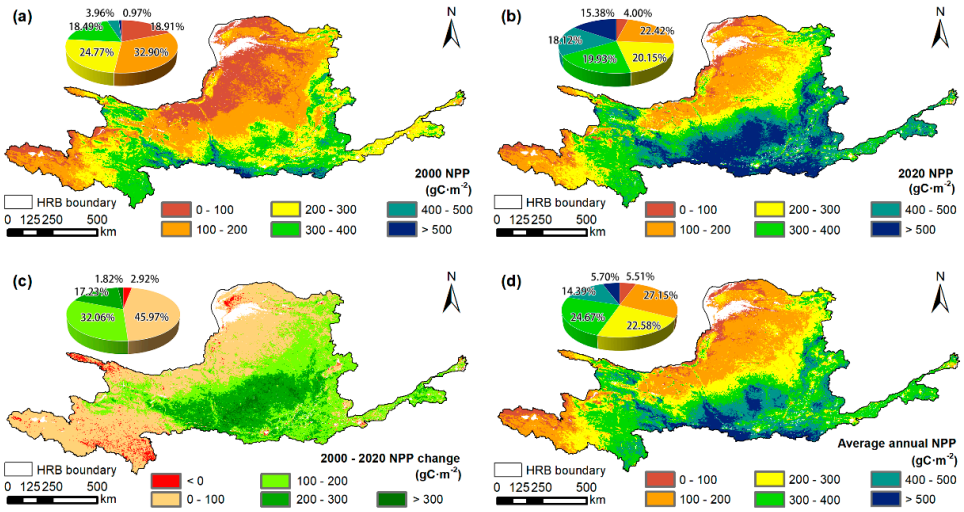


Figure 5. Spatial distribution of NPP in 2000 (**a**), 2020 (**b**), the changes (**c**), and the annual average NPP during 2000–2020 (**d**) in the YRB.

3.2.3. Linear and Nonlinear Trends for NPP

An overview of the spatial pattern of NPP trend during 2000–2020 was presented in Figure 6. For both linear and nonlinear trends, the areas with significantly decreasing NPP were very small (0.28% and 0.29%, respectively). In the case of a linear trend, about 71.43% of the YRB exhibited an ESI trend ($p < 0.01$) and 11.96% showed a SI trend ($p < 0.05$), which were primarily distributed in the central part of the YRB, particularly in the provinces of Shaanxi, Shanxi and Ningxia. Only 16.34% of the regions showed insignificant changes in NPP, mainly distributed in the eastern of Qinghai province and the downstream of the YRB. The area percentage of insignificant variation trends suggested by EEMD was only 1.79%, whereas 16.34% by the linear trend (Figure 6b). The statistically MI trend accounted for 72.77%. The trend reversal of ID and DI occupied the estimated percentage of 3.81% and 21.36%, respectively (Figure 7). The trend of ID was mainly located in the eastern of Qinghai province and Mu Us Sandy Land. The trend of DI was mainly concentrated in the Hetao Plain in central Inner Mongolia. Notably, about 12.12% and 9.10% of the regions showed significant increase ($p < 0.05$) and insignificant change in the linear trend, respectively, but showed a reverse trend of ID in EEMD analysis (Figure 7).

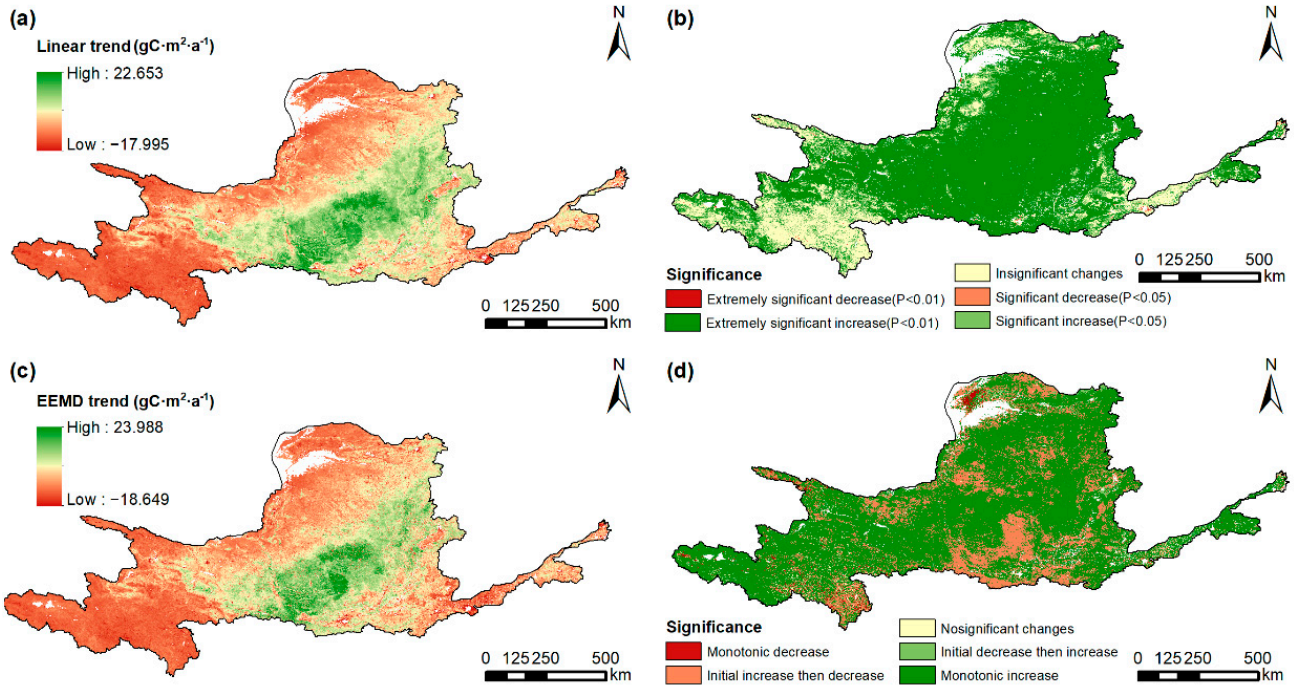


Figure 6. Trends of NPP from 2000 to 2020. The Sen trend (**a**) and its significance classified (**b**); ensemble empirical mode decomposition (EEMD) trend (**c**) and its significance classified (**d**).

For different vegetation types, the proportion of monotonic increase in forests (83.41%) and croplands (86.35%) were higher than that of others (Figure 8). Although the area of MD trend in most vegetation types was low, the area of ID occupied approximately 73.22% in the areas of the whole grassland, and about 27.47% of the whole shrublands.

3.3. Multi-Timescale Analyses for Vegetation NPP

As illustrated in Figure 9 and Table 2, NPP in the YRB was decomposed into three IMF components and one residue based on EEMD. The quasi-periodic fluctuations of the three IMF were expressed as 3-, 6-, and 10.5-year time scales and the residue represented a long-term trend. The IMF1 had the largest variance contribution (VC) (50.73%), followed by the residual (33.54%). The VC values of IMF2 and IMF3 were 13.26% and 2.47%, respectively. Since the value of IMF3 was below 10%, it was discarded in the later analysis (Table 2).

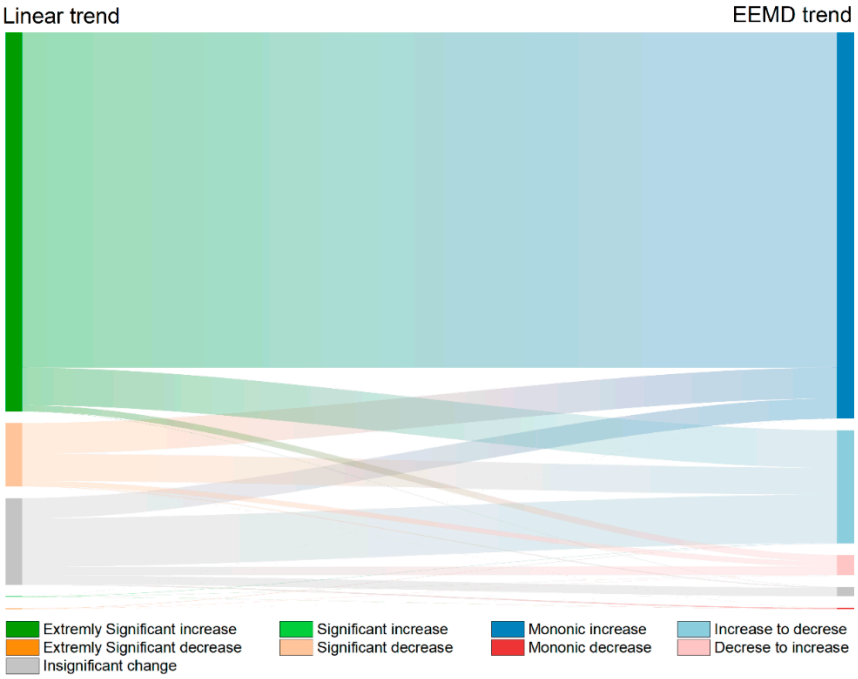


Figure 7. Percentage of area converted from linear trend to EEMD trend (%).

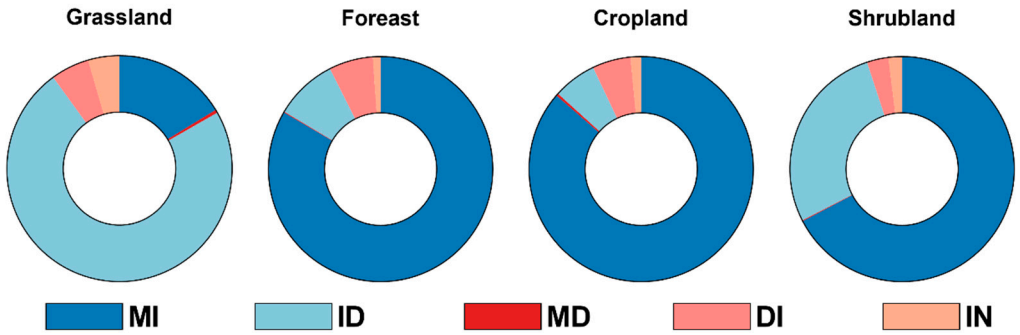


Figure 8. Area percentage (%) of different vegetation types under EEMD trend classification.

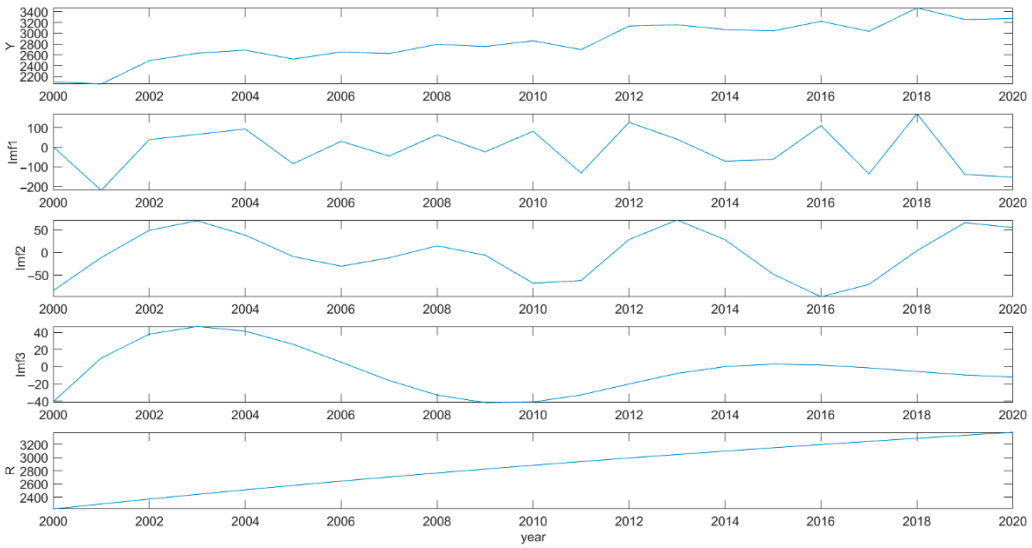


Figure 9. EEMD analysis of the average NPP changes during 2000–2020.

Table 2. Averaged periods of NPP in YRB at different time scales and their variance contributions.

Variable Types	IMF1	IMF2	IMF3	Residue
Period (timescale/a)	3	6	10.5	—
Variance contribution (%)	50.73	13.26	2.47	33.54
Ranking	1	3	4	2

For the 3-year time scale, the regions with VC less than 20% occupied 41.56% of all pixels, which were mainly located in the Shaanxi province and Shanxi province (Figure 10a). However, the areas in the YRB with a VC of more than 40% occupied 30.19%, which were distributed in Hetao Plain and downstream regions of the YRB. For the 6-year time scale, the distribution characteristics of the VC were consistent with those at the 3-year time scale, but with lower values (Figure 10b). The regions with VC values < 8% occupied 61.51%, which were found in eastern parts of the YRB, especially in Shanxi province and the northern part of Shaanxi province. However, the VC values higher than 18% only occupied 12% of the study area. For long-term trends, more than 45% of the study area had VC values higher than 60% (Figure 10d). In most of Shaanxi province and the western part of Shanxi province, the VC was very high (50–90%). The VC values were relatively low in the north of Ningxia, central Inner Mongolia, and the boundary junction of Qinghai, Gansu, and Sichuan provinces, which were relatively high at the 3-year oscillation. Overall, the VC pattern of long-term trend was opposite to the 3-year oscillation.

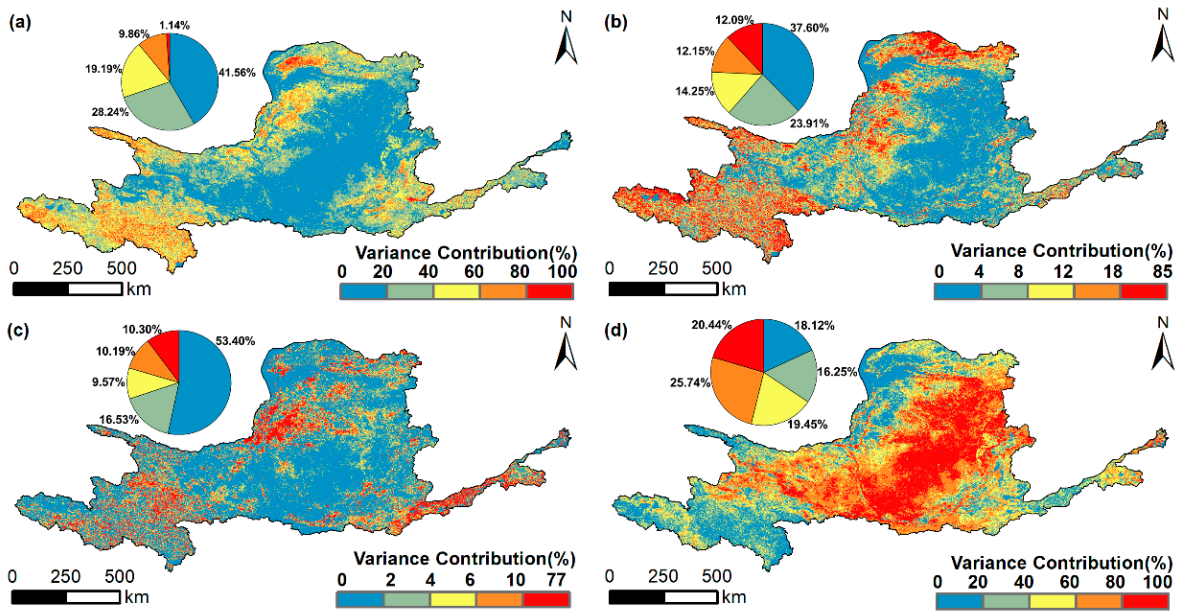


Figure 10. The EEMD analysis of the average NPP during 2000–2020. (**a**–**c**) IMF1–IMF3 and (**d**) residual.

Considering various vegetation types, such as croplands, the VC values of 3-year oscillation are similar to those of the long-term trends (Table 3). Conversely, compared to long-term changes, the VC values of the 3-year oscillation had a greater impact on other vegetation types. At the 3-year oscillation point, the VC of grassland, forest, and shrublands was 52.11%, 55.65%, and 52.96%, respectively. Over the 6-year time scale, the VC values of forest, cropland, and shrublands were below 10%. In addition, the distribution of VC values in grassland exhibited significant heterogeneity and varied across different time scales. Grasslands in the middle reaches of the Yellow River have smaller (below 20%) VC values at short time scales, but relatively larger VC values (above 80%) at long term scales. For forest and shrublands, the VC values exhibited an inverse relationship between the 3-year oscillation and long-term scales.

Table 3. Percentage of variance contribution by vegetation types across different temporal scales (%).

	Grassland	Forest	Cropland	Shrublands
IMF1	52.11	55.65	45.73	52.96
IMF2	10.40	7.56	7.30	8.92
Residue	33.45	33.16	42.72	34.60

3.4. The Temporal Relationships between Vegetation NPP and Various Climatic Factors

3.4.1. Multiple Time Scale Analysis for Meteorological Factors

To elucidate the correlations between NPP and meteorological factors at different time scales, the mean temperature and precipitation between 2000 and 2020 were decomposed in to three oscillations and one residual based on the EEMD method (Figure 11). The mean temperature was separated into 3-, 6-, and 20-year oscillations in the study area, and the VC values of IMF1 and IMF2 were identical (Figure 11 and Table 4). The annual precipitation was separated into 3-, 6-, and 21-year oscillations, and the average VC value of IMF1 was 79.27%, which was larger than other IMFs. In the long-term trend, the temperature increased gradually, while the precipitation showed a trend of DI (Table 4).

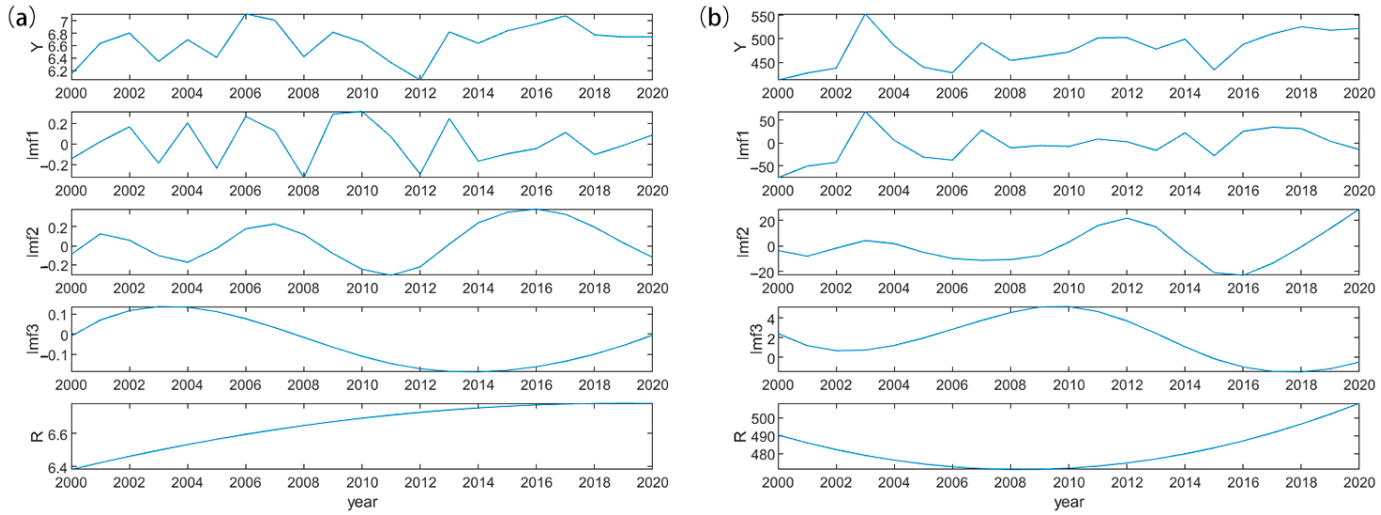


Figure 11. IMFs and residue of annual average temperature (**a**) and annual precipitation (**b**) during 2000–2020.

Table 4. The variance contributions (VC) and mean periods of climate factors across different time scales.

		IMF1	IMF2	IMF3	Residue
Temperature	Period (timescale/a)	3	6	20	—
	Variance contribution (%)	35.37	32.31	13.90	17.43
	Ranking	1	2	4	3
Precipitation	Period (timescale/a)	3	6	21	—
	Variance contribution (%)	79.27	12.60	0.39	7.74
	Ranking	1	2	4	3

3.4.2. Possible Relationships between NPP and Climate Factors at Different Time Scales

During the study period, a correlation analysis was conducted at the pixel scale to investigated the correlation between NPP and meteorological factors across multiple time spans (Figures 12 and 13). At the 3-year oscillation, NPP had an insignificant correlation with temperature for most study areas (more than 97%) (Figure 12a). The areas of negative correlation between temperature and NPP were in the downstream of the YRB, and were

mainly composed of croplands and grassland. The relationship of vegetation NPP and precipitation had spatial heterogeneity (Figure 12b). About 86.99% of all pixels showed a moderate intensity correlation between precipitation and vegetation NPP, and the proportion of the study area with statistically significant positive correlation ($p < 0.05$) extended to 41.54%. The concentration of this region is primarily observed in the northern section of the Yellow River basin. At the 6-year temporal scale, the correlation between NPP and temperature with moderate intensity ($|r| > 0.4$) accounted for only 11.66% (Figure 12c). The relationship between vegetation NPP and precipitation was found to be negative in the downstream of the YRB. In more than 77% of the YRB, NPP was positive correlated with precipitation, and the areas of significant positive correlation decreased from 41.54% to 8.67%, which were found in the arid and semi-arid regions of the northern Loess Plateau (Figure 12d). Conversely, a negative relationship was observed in the downstream regions of the YRB, constituting 36.32% of all pixels. The long-term trend revealed a positive correlation between NPP and temperature in the source regions of the YRB (Figure 12e). The areas of significant positive correlation increased from 0.71% to 11.57%, which were primarily located in the eastern region of Qinghai province with high elevation. Long-term increase in temperature may be a primary factor influencing the growth of NPP in alpine regions. The positive relationship between precipitation and vegetation NPP occupied more than 53% of all pixels (Figure 12f). In particular, 48.21% of all pixels showed a positive correlation with precipitation under significance, primarily located in the northern Loess Plateau and plain areas downstream of the YRB.

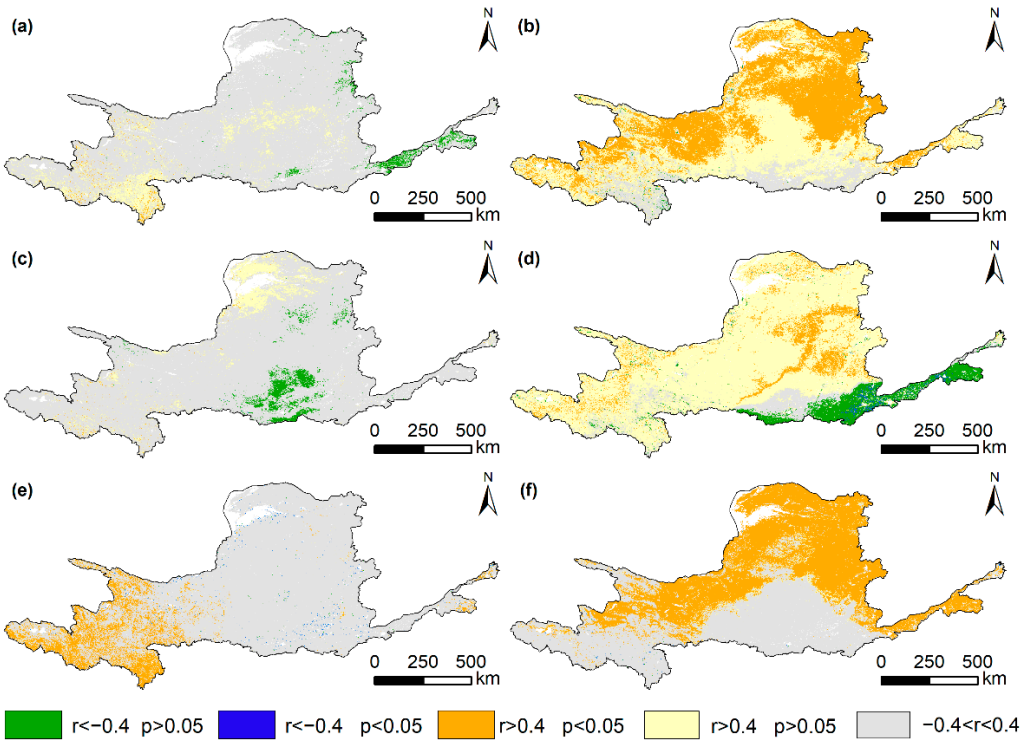


Figure 12. Relationships between NPP and temperature (**a**,**c**,**e**), and the relationships with precipitation (**b**,**d**,**f**) at 3- and 6-year time scales and overlong term trend in YRB (r: correlation coefficient; *p*: significance level).

In the short-term scale, the positive response of NPP to precipitation was significant (3 year: 31.6%; 6 year: 9.73%). For shrubs, temperature and precipitation were similar to the positive and negative correlation areas with NPP. On the 6-year scale, the NPP of forest land was negatively correlated with temperature. On a long-term scale, all vegetation types were positively correlated with hydrothermal factors. Among them, NPP showed

a positive correlation with temperature and precipitation in more than 80% of the areas (Figure 14).

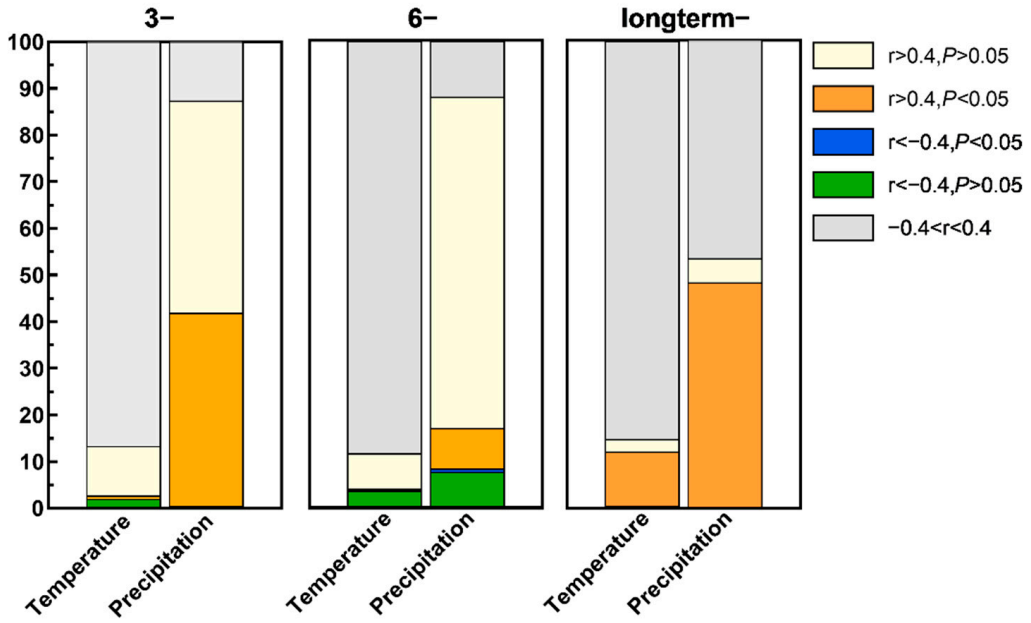


Figure 13. Percentage of study areas for correlation between NPP and climate factors across different time scales (%).

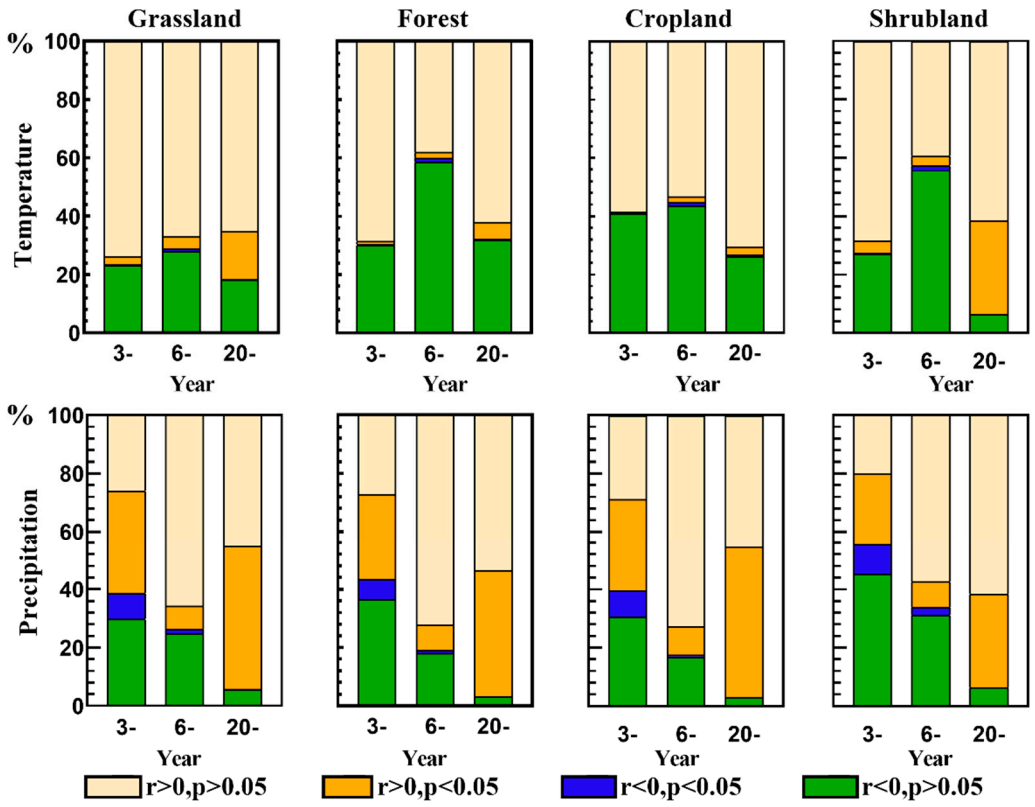


Figure 14. Percentage of areas for correlation between NPP and climate factors in different vegetation types (%).

3.5. The Relative Contributions of Climate Changes and Human Activities to Vegetation NPP across Multiple Time Scales

In this study, a multivariate regression (MLR) model was adopted for NPP based on the annual temperature and precipitation. Furthermore, to reveal the relative importance of climate changes and anthropogenic activities to NPP with multiple time spans, the IMF components of NPP and its driving factors were also used to establish the MLR (Figure 15).

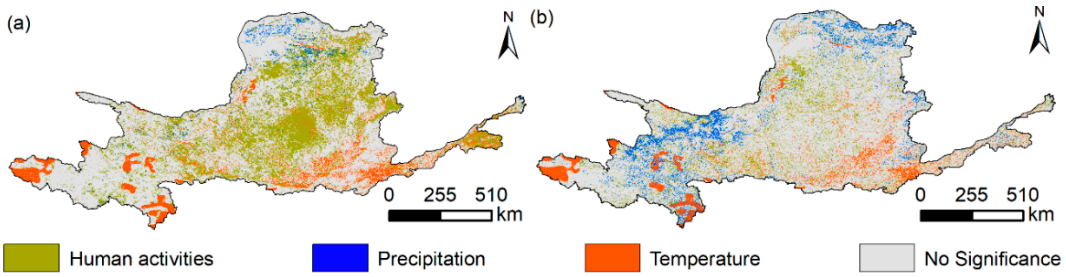


Figure 15. Spatial distribution characteristic of the dominant drivers for NPP change under the MLR model. (**a**) Without multiple time scale analysis; (**b**) with multiple time scale analysis.

Without multiple time scales, about 11.94% of the study area demonstrates statistical significance in the test ($p < 0.05$). The areas where NPP was dominated by precipitation and temperature occupied 0.58% and 2.95% of all pixels, respectively. Regions with human-activity-dominated NPP were mostly located in Shaanxi and Shanxi provinces and the cropland regions downstream of the YRB, accounting for 8.41% of all pixels. With multiple time scales, the proportion of areas with significance was 11.44%. The regions where NPP was dominated by temperature and precipitation occupied 3.43% and 2.13% of all pixels, respectively. The regions where NPP was controlled by human activities only occupied 5.88% of the study area, which was similar to climate-dominated areas. For different vegetation types, the NPP of 15.4% of cultivated land was dominated by temperature. Climate was the main factor affecting NPP in grassland, and only 15.74% of the grassland was affected by human activities. For shrublands, forests, and croplands, human activities are still an important factor influencing their NPP changes.

4. Discussion

4.1. Nonlinear Trends of Vegetation NPP Dynamics

The nonlinear trend analysis method is helpful to better comprehend the vegetation dynamics and its correlation with climate change [24,48]. Our findings indicate that the vegetation NPP increased over the past two decades in the YRB, which is in line with the research conducted by Tian et al. [41], who determined that the increasing rate of NPP was 2.35 g C m^{-2} a^{-1} during 1982–2020 in the YRB. According to our research, vegetation NPP had a significant rising trend in both linear (83.39%) and nonlinear (72.77%) trend methods in the YRB from 2000 to 2020, which was consistent with what was reported in previous research [27,49]. Remarkably, the EEMD method can not only detect the significance in the change trends, in the same way as the method of linear trend, but also reveal the reversal of trends [23]. The significant increase and no significant change of NPP by linear trend occupied 12.12% and 9.10% of all pixels, but showed an initial decrease then increase by EEMD analysis. This finding indicates that linear trends ignore the reversal trend of NPP, which might underestimate or overestimate the risk of vegetation degradation [17]. Thus, revealing the reversal trend was essential to characterize the trends of NPP accurately [9].

The area of NPP trend of DI was only 3.81% of all pixels, especially in the north of the YRB. Previous research demonstrated that the degradation of vegetation in central Inner Mongolia caused by arid climatic conditions has been mitigated through sufficient moisture and effective ecological engineering programs, which might reverse the decline in NPP [13]. This study also indicates that the trend of ID in NPP reached 49.42% of all pixels, especially in the eastern region of Qinghai province. Previous studies reported that

the grassland NPP had shifted from an increasing to decreasing trend after 2001 in the west of Qinghai Province [8,28], which matches with our results. Meanwhile, our findings also exhibit that the NPP trend reversed in the Mu Us sandy land during 2000–2020. On the one hand, we inferred that the adverse effects of over-restoration and water deficiency played an essential role in causing the reversal of NPP trend [30,34]. With global warming, vegetation greening will inevitably exacerbate the regional ecological water pressure in arid and semi-arid areas [5,25]. Although vegetation restoration had a positive impact on the ecological environments of the Mu Us sandy land, the soil moisture evapotranspiration was aggravated due to the vegetation greening [59]. Thus, we should pay more attention to avoid expanding vegetation cover without considering the water consumption capacity of vegetation for ecological restoration projects in the future. On the other hand, the period of this study only covered the past 2 decades, following successful implementation of the Grain to Green Program, which possibly led to the shifts in NPP trends [37,43]. Overall, it is critical to study the reversal trends of NPP changes to give timely alerts for future vegetation variation and develop corresponding strategies for vegetation restoration.

4.2. Effects of Climate Change of Vegetation NPP across Multi-Time Scales

Previous studies showed that the vegetation variations were not only affected by hydrothermal conditions [37,60], elevation [12], and vegetation types [9], but they also vary with time scales [18]. We observed that the NPP dynamics were primarily influenced by 3-year oscillation and the long-term trend, which was in line with the results reported by Liu et al. [12] in karst regions of southwest China. Specifically, the NPP dynamics were affected by the 3-year time scale with elevation above 3000 m in the YRB. One possible explanation was that vegetation condition was easily affected by climate changes and anthropogenic disruptions in a short-term period in the alpine region due to the delicate ecological environments and harsh climatic conditions [39]. Additionally, the long-term trend exhibited a higher VC than that of the 3-year oscillation in middle areas of the YRB with elevation below 1500 m, especially in Shaanxi and Shanxi provinces, which can be attributed to the mitigation of the vegetation degradation under long-term ecological restoration measures [2]. Meanwhile, our results found the VC of 3-year oscillation was in line with that of the long-term trend in the downstream area of the YRB dominated by croplands, indicating that both 3-year oscillations and long-term trend were dominant time scales for croplands. This may be attributed to human agricultural planning, resulting in the stable variation in NPP [13].

Our findings also confirm that the relationships between vegetation NPP and meteorological change are sensitive to temporal scales and are primarily determined by a combination of vegetation types, elevation, and hydrothermal conditions. In short time scales (3 and 6 years), vegetation change in arid and semi-arid regions exhibited an inverse correlation with temperature, albeit with less statistical significance, which was in line with previous findings [12]. In some areas with scarce water resources, a short-term increase in temperature can accelerate soil moisture evaporation, which inhibits the vegetation growth [25,30]. However, as the time scale widens, an obvious spatial heterogeneity in the relationship between NPP and temperature becomes apparent. Vegetation NPP significantly grew with rising temperature in the long-term trend, particularly in the region with altitude above 3000 m (Figure 10). Temperature is the primary climatic factor limiting vegetation growth in the alpine region, and long-term warming may promote photosynthetic efficiency and be beneficial to vegetation growing [59,61]. The relationship between precipitation and NPP showed obvious spatial heterogeneity. At the 3-year oscillation, the NPP exhibited a positive correlation with precipitation in regions with annual precipitation below 400 mm, but a negative correlation in regions with precipitation >600 mm (Figure 10). However, the areas with this significant relationship in short time scales were fewer than those observed over the long-term trend [16,38]. In our study, the long-term trend was found to have strengthened the significance of the relationship between NPP dynamics and climate factors. The impact of climate change on NPP dynamics has become increas-

ingly evident with the widening of the temporal span. These findings indicate that the dependence of vegetation in arid and semi-arid areas is more pronounced on long-term precipitation rather than on short-term precipitation [10]. In addition, the relationship between vegetation NPP and climate factors is also influenced by vegetation type. In the northwest of the Loess Plateau, the water condition is very bad, and the shrub and grassland are the main vegetation types, and the water is the main factor limiting the growth of vegetation. The decrease in precipitation will increase temperature and evapotranspiration, and the grassland and shrubland distributed here will decrease their ecosystem productivity with the decrease in precipitation [62]. The temperature dominated NPP changes mainly in the upper and lower reaches of the Yellow River. The upstream elevation is higher, and temperature becomes the main factor that dominates the NPP change here. The lower reaches are the main farming areas in the Yellow River Basin. Croplands have sufficient water and nutrients to meet their growth needs, which are mainly regulated by temperature under the artificial irrigation [63,64].

4.3. The Effects of Human Activities on Vegetation NPP across Multi-Time Scales

Human activities are also critical drivers of NPP changes [15,65]. Although many reports have distinguished the effects of meteorological factors and human factors on vegetation [4], there are few studies linking them with time scales in the Yellow River Basin. In this study, time scale is introduced into multiple linear regression analysis, which is very important to uncover the hidden relationship between vegetation NPP and climate and human factors in the Yellow River Basin. The impact of anthropogenic activities on vegetation was more pronounced than that of climate change in the aforementioned regions. Climate factors had a limited influence on NPP without multi-time scales [18]. In this work, we found that temperature and precipitation dominated larger areas with significance across multi-time scales (Figure 11). Meanwhile, the areas affected by climatic and anthropogenic activities are similar. In different vegetation types, the area of grassland affected by human activities is much smaller than that of the area dominated by climate factors, which may be due to the short root system of grassland and its obvious response to temperature and precipitation change. For shrubland, forest, and cultivated land, human activities are still the important factors affecting the change in NPP. Thus, exploring the relative significance of vegetation, climate, and anthropogenic factors across multiple temporal scales can offer crucial guidance for the implementation of future vegetation restoration projects.

4.4. Limitation and Future Work

In this study, based on the EEMD method, the nonlinear change in vegetation NPP in the Yellow River Basin was investigated. No discernible periodicity was observed in the long-term nonlinear trend, potentially attributed to the relatively short duration of the study period, spanning only 20 years. Using longer time series in future studies may lead to regular cycles. In addition, the oscillation period obtained based on the decomposition of the EEMD model in this study is carried out on the annual scale. Higher time resolution, such as monthly and seasonal resolution, may be helpful for the study of the periodic changes in vegetation NPP on multiple time scales.

For driving factors, although we have examined the temporal scales of climate and anthropogenic factors' relative contributions, it remains unclear how this relationship varies at different time scales. Moreover, the factors affecting vegetation changes are complex [5]. Previous studies have shown that solar radiation [32], CO_2 [65], extreme climate [66], and other factors also affect the changes in vegetation NPP. Consideration of multiple driving factors in future studies will facilitate a more thorough comprehension of the response mechanisms of vegetation to climate change.

Additionally, only a simple correlation analysis was used to characterize the relationship between vegetation NPP and climate factors in this study, which may introduce uncertainty and limit further exploration of this association. Future research should focus

on land surface models that can explain this relationship scientifically. Moreover, the investigation into the primary motivators of human activities lacks sufficient detail at present, and future studies should consider the influence of specific anthropogenic activities on vegetation NPP, such as urban construction and ecological restoration projects.

Moreover, the land-use type was assumed to remain unchanged from 2000 to 2020 in this study, while disregarding the potential impact of changes in land-use type on vegetation NPP. Therefore, our study assumes no change in vegetation types from 2000 to 2020, which may lead to uncertainty in NPP analysis in the YRB, because vegetation in the Yellow River Basin has been affected by ecological restoration projects, and vegetation types have changed in the past 20 years. Therefore, future studies should aim to consider what will happen to NPP as vegetation types change.

5. Conclusions

In this study, we investigated the upward trend of NPP and potential multiple time scales of NPP changes were examined with the EEMD method from 2000 to 2020 in the YRB. The mean annual NPP was 236.37 g C/m^2 in the YRB from 2000 to 2020. The EEMD analysis revealed that 72.77% of the YRB exhibited a monotonically increasing trend in NPP. The regions exhibiting a shift in the trend of vegetation NPP from an increase to a decrease were predominantly observed within the Mu Us sandy land and the western alpine area of the YRB. The vegetation NPP changes were controlled by 3-year oscillation and long-term trend. Cropland was impacted by a combination of both short- and long-term time scales, and grassland was primarily distinguished by its 3-year temporal scale. The relationship between NPP dynamics and climate change at different time scales shows obvious an spatial heterogeneity pattern. Temperature was negatively correlated with NPP at short time scales in semi-arid and arid regions, and this relationship reversed with increasing time scales. Vegetation NPP was more dependent on precipitation over the long-term trend. Regarding the correlation of NPP and climate factors, areas that exhibited significance were more pronounced as the time span widened. The impact of anthropic activities on vegetation dynamics was regionally different. The climate factors had a limited influence on NPP without multiple timescales. Due to the large area and the differences in climatic conditions and topography, the dominant factor influencing the NPP in the YRB has obvious spatial heterogeneity. Temperature dominates the vegetation dynamics in the source area of the Yellow River at high altitudes, and precipitation is the dominant factor in the arid areas lacking in water, and the region of human activities is scattered, mainly distributed in the middle of the basin or the lower reaches of the Yellow River. However, in general, climate factors are still the main factors affecting NPP variation in vegetation in the YRB. Among different vegetation types, climate factors were the main factors affecting grassland NPP. For shrubland, forest, and farmland, human activity was an important factor affecting the change in NPP. The utilization of nonlinear trend analysis and multiple timescale analysis can facilitate the identification of NPP trend reversals as well as the assessment of climate change impacts on NPP variability, thereby enabling revealed the hidden relationship between vegetation NPP and climate and human factors across time scales. Our work will provide Chinese government agencies with informed decision-making on the future protection of vegetation in the YRB.

Supplementary Materials: The following supporting information can be downloaded at: https://www.mdpi.com/article/10.3390/rs15225273/s1, Figure S1: The distribution of 722 meteorological stations; Figure S2: Relationship between MOD17A3 NPP and BIOME-BGC NPP, LUE NPP estimation; Figure S3: Spatial patterns and trends of driving factors.

Author Contributions: Conceptualization and supervision: Y.L. and C.Z.; design and methodology: Y.L. and Z.L.; data analysis: X.C., Z.W. (Zijun Wang), P.H. and C.Z.; data curation: H.S., Z.W. (Zhongming Wen) and H.Y.; writing—original draft preparation: Y.L. and Z.L.; writing—review and editing: Z.W. (Zhongming Wen) and H.S. All authors have read and agreed to the published version of the manuscript.

Funding: This work was supported by the National Natural Science Foundation of China (No. 42107512 and No. 41977077), the "Open Foundation of the Key Laboratory of Coupling Process and Effect of Natural Resources Elements" (No. 2022KFKTC004), the "Open Foundation of Yinshanbeilu Grassland Eco-Hydrology National Observation and Research Station, China Institute of Water Resources and Hydropower Research, Beijing 100038, China" (No. YSS2022009), and the "Special project of science and technology innovation plan of Shaanxi Academy of Forestry Sciences" (No. SXLK2022–02-7 and No. SXLK2023–02-14).

Data Availability Statement: Data will be made available on request.

Acknowledgments: We acknowledge the data support from "Loess plateau science data center, National Earth System Science Data Sharing Infrastructure, National Science & Technology Infrastructure of China (http://loess.geodata.cn, accessed on 18 January 2023)".

Conflicts of Interest: The authors declare no conflict of interest.

References

1. Legg, S. IPCC, 2021: Climate change 2021-the physical science basis. *Interaction* **2021**, *49*, 44–45.
2. Chang, J.; Liu, Q.; Wang, S.; Huang, C. Vegetation Dynamics and Their Influencing Factors in China from 1998 to 2019. *Remote Sens.* **2022**, *14*, 3390. [CrossRef]
3. Jian, S.Q.; Zhang, Q.K.; Wang, H.L. Spatial-Temporal Trends in and Attribution Analysis of Vegetation Change in the Yellow River Basin, China. *Remote Sens.* **2022**, *14*, 4607. [CrossRef]
4. Zhou, X.; Peng, B.; Zhou, Y.; Yu, F.; Wang, X.-C. Quantifying the Influence of Climate Change and Anthropogenic Activities on the Net Primary Productivity of China's Grasslands. *Remote Sens.* **2022**, *14*, 4844. [CrossRef]
5. Liu, H.; Jia, J.; Lin, Z.; Wang, Z.; Gong, H. Relationship between net primary production and climate change in different vegetation zones based on EEMD detrending—A case study of Northwest China. *Ecol. Indic.* **2021**, *122*, 107276. [CrossRef]
6. Zhang, F.; Hu, X.S.; Zhang, J.; Li, C.Y.; Zhang, Y.P.; Li, X.L. Change in Alpine Grassland NPP in Response to Climate Variation and Human Activities in the Yellow River Source Zone from 2000 to 2020. *Sustainability* **2022**, *14*, 8790. [CrossRef]
7. Field, C.B.; Behrenfeld, M.J.; Randerson, J.T.; Falkowski, P. Primary production of the biosphere: Integrating terrestrial and oceanic components. *Science* **1998**, *281*, 237–240. [CrossRef]
8. Xue, P.; Liu, H.; Zhang, M.; Gong, H.; Cao, L. Nonlinear Characteristics of NPP Based on Ensemble Empirical Mode Decomposition from 1982 to 2015-A Case Study of Six Coastal Provinces in Southeast China. *Remote Sens.* **2022**, *14*, 15. [CrossRef]
9. Gong, H.B.; Cao, L.; Duan, Y.F.; Jiao, F.S.; Xu, X.J.; Zhang, M.Y.; Wang, K.L.; Liu, H.Y. Multiple effects of climate changes and human activities on NPP increase in the Three-north Shelter Forest Program area. *For. Ecol. Manag.* **2023**, *529*, 120732. [CrossRef]
10. Chen, T.; Tang, G.; Yuan, Y.; Guo, H.; Xu, Z.; Jiang, G.; Chen, X. Unraveling the relative impacts of climate change and human activities on grassland productivity in Central Asia over last three decades. *Sci Total Env.* **2020**, *743*, 140649. [CrossRef]
11. Wang, B.; Sun, R.; Deng, Y.; Zhu, H.; Hou, M. The Variability of Net Primary Productivity and Its Response to Climatic Changes Based on the Methods of Spatiotemporal Decomposition in the Yellow River Basin, China. *Pol. J. Environ. Stud.* **2022**, *31*, 4229–4312. [CrossRef] [PubMed]
12. Liu, H.; Zhang, M.; Lin, Z. Relative importance of climate changes at different time scales on net primary productivity-a case study of the Karst area of northwest Guangxi, China. *Env. Monit Assess* **2017**, *189*, 539. [CrossRef]
13. Liang, W.; Yang, Y.T.; Fan, D.M.; Guan, H.D.; Zhang, T.; Long, D.; Zhou, Y.; Bai, D. Analysis of spatial and temporal patterns of net primary production and their climate controls in China from 1982 to 2010. *Agric. For. Meteorol.* **2015**, *204*, 22–36. [CrossRef]
14. Hawinkel, P.; Swinnen, E.; Lhermitte, S.; Verbist, B.; Van Orshoven, J.; Muys, B. A time series processing tool to extract climate-driven interannual vegetation dynamics using Ensemble Empirical Mode Decomposition (EEMD). *Remote Sens. Environ.* **2015**, *169*, 375–389. [CrossRef]
15. Ghorbanian, A.; Mohammadzadeh, A.; Jamali, S. Linear and Non-Linear Vegetation Trend Analysis throughout Iran Using Two Decades of MODIS NDVI Imagery. *Remote Sens.* **2022**, *14*, 3683. [CrossRef]
16. Cao, R.; Hu, Z.; Jiang, Z.; Yang, Y.; Zhao, W.; Wu, G.; Feng, X.; Chen, R.; Hao, G. Shifts in ecosystem water use efficiency on china's loess plateau caused by the interaction of climatic and biotic factors over 1985–2015. *Agric. For. Meteorol.* **2020**, *291*, 108100. [CrossRef]
17. Cui, J.; Wang, Y.; Zhou, T.; Jiang, L.; Qi, Q. Temperature Mediates the Dynamic of MODIS NPP in Alpine Grassland on the Tibetan Plateau, 2001–2019. *Remote Sens.* **2022**, *14*, 2401. [CrossRef]
18. Ma, B.; Jing, J.; Liu, B.; Xu, Y.; Dou, S.; He, H. Quantitative assessment of the relative contributions of climate change and human activities to NPP changes in the Southwest Karst area of China. *Environ. Sci. Pollut. Res.* **2022**, *29*, 80597–80611. [CrossRef]
19. Song, Y.; Liang, T.; Zhang, L.; Hao, C.; Wang, H. Spatio-Temporal Changes and Contribution of Human and Meteorological Factors to Grassland Net Primary Productivity in the Three-Rivers Headwater Region from 2000 to 2019. *Atmosphere* **2023**, *14*, 278. [CrossRef]
20. Chen, B.; Zhang, X.; Tao, J.; Wu, J.; Wang, J.; Shi, P.; Zhang, Y.; Yu, C. The impact of climate change and anthropogenic activities on alpine grassland over the Qinghai-Tibet Plateau. *Agric. For. Meteorol.* **2014**, *189–190*, 11–18. [CrossRef]

21. Shi, S.Y.; Yu, J.J.; Wang, F.; Wang, P.; Zhang, Y.C.; Jin, K. Quantitative contributions of climate change and human activities to vegetation changes over multiple time scales on the Loess Plateau. *Sci. Total Environ.* **2021**, *755*, 142419. [CrossRef]
22. Zhao, L.; Liu, Z.; Hu, Y.; Zhou, W.; Peng, Y.; Ma, T.; Liu, L.; Li, S.; Wang, L.; Mao, X. Evaluation of Reasonable Stocking Rate Based on the Relative Contribution of Climate Change and Grazing Activities to the Productivity of Alpine Grasslands in Qinghai Province. *Remote Sens.* **2022**, *14*, 1455. [CrossRef]
23. Xu, X.J.; Jiao, F.S.; Liu, H.Y.; Gong, H.B.; Zou, C.X.; Lin, N.F.; Xue, P.; Zhang, M.Y.; Wang, K.L. Persistence of increasing vegetation gross primary production under the interactions of climate change and land use changes in Northwest China. *Sci. Total Environ.* **2022**, *834*, 155086. [CrossRef] [PubMed]
24. Xuan, W.; Rao, L. Spatiotemporal dynamics of net primary productivity and its influencing factors in the middle reaches of the Yellow River from 2000 to 2020. *Front. Plant Sci.* **2023**, *14*, 1043807. [CrossRef] [PubMed]
25. Xu, X.J.; Liu, H.Y.; Jiao, F.S.; Gong, H.B.; Lin, Z.S. Nonlinear relationship of greening and shifts from greening to browning in vegetation with nature and human factors along the Silk Road Economic Belt. *Sci. Total Environ.* **2021**, *766*, 142553. [CrossRef] [PubMed]
26. Ji, Y.; Zhou, G.; Wang, S.; Wang, L. Prominent vegetation greening and its correlation with climatic variables in northern China. *Environ. Monit. Assess.* **2020**, *192*, 636. [CrossRef] [PubMed]
27. Liu, H.Y.; Zhang, M.Y.; Lin, Z.S.; Xu, X.J. Spatial heterogeneity of the relationship between vegetation dynamics and climate change and their driving forces at multiple time scales in Southwest China. *Agric. For. Meteorol.* **2018**, *256*, 10–21. [CrossRef]
28. Zhang, W.; Wang, L.C.; Xiang, F.F.; Qin, W.M.; Jiang, W.X. Vegetation dynamics and the relations with climate change at multiple time scales in the Yangtze River and Yellow River Basin, China. *Ecol. Indic.* **2020**, *110*, 105892. [CrossRef]
29. Tian, F.; Liu, L.Z.; Yang, J.H.; Wu, J.J. Vegetation greening in more than 94% of the Yellow River Basin (YRB) region in China during the 21st century caused jointly by warming and anthropogenic activities. *Ecol. Indic.* **2021**, *125*, 107479. [CrossRef]
30. Hong, S.; Zhang, Y.; Yao, Y.; Meng, F.; Zhao, Q.; Zhang, Y. Contrasting temperature effects on the velocity of early- versus late-stage vegetation green-up in the Northern Hemisphere. *Glob. Chang. Biol.* **2022**, *28*, 6961–6972. [CrossRef]
31. Hu, Y.G.; Li, H.; Wu, D.; Chen, W.; Zhao, X.; Hou, M.L.; Li, A.J.; Zhu, Y.J. LAI-indicated vegetation dynamic in ecologically fragile region: A case study in the Three-North Shelter Forest program region of China. *Ecol. Indic.* **2021**, *120*, 106932. [CrossRef]
32. Wu, Z.; Huang, N.E. Ensemble empirical mode decomposition: A noise-assisted data analysis method. *Adv. Adapt. Data Anal.* **2009**, *1*, 1–41. [CrossRef]
33. Kong, D.; Zhang, Q.; Singh, V.P.; Shi, P. Seasonal vegetation response to climate change in the Northern Hemisphere (1982–2013). *Glob. Planet. Chang.* **2017**, *148*, 1–8. [CrossRef]
34. Xue, Y.Y.; Zhang, B.Q.; He, C.S.; Shao, R. Detecting Vegetation Variations and Main Drivers over the Agropastoral Ecotone of Northern China through the Ensemble Empirical Mode Decomposition Method. *Remote Sens.* **2019**, *11*, 1860. [CrossRef]
35. Feng, Y.; Zhu, J.; Zhao, X.; Tang, Z.; Zhu, J.; Fang, J. Changes in the trends of vegetation net primary productivity in China between 1982 and 2015. *Environ. Res. Lett.* **2019**, *14*, 124009. [CrossRef]
36. Wei, F.L.; Wang, S.; Fu, B.J.; Pan, N.Q.; Feng, X.M.; Zhao, W.W.; Wang, C. Vegetation dynamic trends and the main drivers detected using the ensemble empirical mode decomposition method in East Africa. *Land Degrad. Dev.* **2018**, *29*, 2542–2553. [CrossRef]
37. Yin, Y.X.; Xu, C.Y.; Chen, H.S.; Li, L.; Xu, H.L.; Li, H.; Jain, S.K. Trend and concentration characteristics of precipitation and related climatic teleconnections from 1982 to 2010 in the Beas River basin, India. *Glob. Planet. Chang.* **2016**, *145*, 116–129. [CrossRef]
38. Ren, Z.G.; Tian, Z.H.; Wei, H.T.; Liu, Y.; Yu, Y.P. Spatiotemporal evolution and driving mechanisms of vegetation in the Yellow River Basin, China during 2000–2020. *Ecol. Indic.* **2022**, *138*, 108832. [CrossRef]
39. Guo, X.; Tong, S.; Ren, J.; Ying, H.; Bao, Y. Dynamics of Vegetation Net Primary Productivity and Its Response to Drought in the Mongolian Plateau. *Atmosphere* **2021**, *12*, 1587. [CrossRef]
40. Xiao, F.; Liu, Q.; Xu, Y. Estimation of Terrestrial Net Primary Productivity in the Yellow River Basin of China Using Light Use Efficiency Model. *Sustainability* **2022**, *14*, 7399. [CrossRef]
41. Tian, H.W.; Ji, X.J.; Zhang, F.M. Spatiotemporal Variations of Vegetation Net Primary Productivity and Its Response to Meteorological Factors across the Yellow River Basin During the Period 1981–2020. *Front. Environ. Sci.* **2022**, *10*, 949564. [CrossRef]
42. Chen, S.; Zhang, Q.; Chen, Y.; Zhou, H.; Xiang, Y.; Liu, Z.; Hou, Y. Vegetation Change and Eco-Environmental Quality Evaluation in the Loess Plateau of China from 2000 to 2020. *Remote Sens.* **2023**, *15*, 424. [CrossRef]
43. Zhang, Y.; Hu, Q.; Zou, F. Spatio-Temporal Changes of Vegetation Net Primary Productivity and Its Driving Factors on the Qinghai-Tibetan Plateau from 2001 to 2017. *Remote Sens.* **2021**, *13*, 1566. [CrossRef]
44. Turner, D.P.; Ritts, W.D.; Cohen, W.B.; Gower, S.T.; Running, S.W.; Zhao, M.S.; Costa, M.H.; Kirschbaum, A.A.; Ham, J.M.; Saleska, S.R.; et al. Evaluation of MODIS NPP and GPP products across multiple biomes. *Remote Sens. Environ.* **2006**, *102*, 282–292. [CrossRef]
45. Zhao, M.S.; Running, S.W. Drought-Induced Reduction in Global Terrestrial Net Primary Production from 2000 through 2009. *Science* **2010**, *329*, 940–943. [CrossRef] [PubMed]
46. Jiang, T.; Wang, X.L.; Afzal, M.M.; Sun, L.; Luo, Y. Vegetation Productivity and Precipitation Use Efficiency across the Yellow River Basin: Spatial Patterns and Controls. *Remote Sens.* **2022**, *14*, 5074. [CrossRef]
47. Yang, H.F.; Zhong, X.N.; Deng, S.Q.; Xu, H. Assessment of the impact of LUCC on NPP and its influencing factors in the Yangtze River basin, China. *Catena* **2021**, *206*, 105542. [CrossRef]
48. Sen, P.K. Estimates of the regression coefficient based on Kendall's tau. *J. Am. Stat. Assoc.* **1968**, *63*, 1379–1389. [CrossRef]

49. Mann, H.B. Nonparametric tests against trend. *Econom. J. Econom. Soc.* **1945**, *13*, 245–259. [CrossRef]
50. Kendall, M. Rank Correlation Methods. Charles Grifin, London. *Ref. Sci. Res. Publishing. Retrieved March* **1975**, *31*, 2020.
51. Yan, X.; Li, J.; Shao, Y.; Hu, Z.; Yang, Z.; Yin, S.; Cui, I. Driving forces of grassland vegetation changes in Chen Barag Banner, Inner Mongolia. *Gisci. Remote Sens.* **2020**, *57*, 753–769. [CrossRef]
52. Sun, Z.; Mao, Z.; Yang, L.; Liu, Z.; Han, J.; Wanag, H.; He, W. Impacts of climate change and afforestation on vegetation dynamic in the Mu Us Desert, China. *Ecol. Indic.* **2021**, *129*, 108020. [CrossRef]
53. Jiang, Z.Y.; Yang, Z.G.; Zhang, S.Y.; Liao, C.M.; Hu, Z.M.; Cao, R.C.; Wu, H.W. Revealing the spatio-temporal variability of evapotranspiration and its components based on an improved Shuttleworth-Wallace model in the Yellow River Basin. *J. Environ. Manag.* **2020**, *262*, 110310. [CrossRef]
54. Shi, S.Y.; Wang, P.; Yu, J.J. Vegetation greening and climate change promote an increase in evapotranspiration across Siberia. *J. Hydrol.* **2022**, *610*, 127965. [CrossRef]
55. Wang, Z.; Dong, C.; Dai, L.; Wang, R.; Liang, Q.; He, L.; Wei, D. Spatiotemporal evolution and attribution analysis of grassland NPP in the Yellow River source region, China. *Ecol. Inform.* **2023**, *76*, 102135. [CrossRef]
56. Zhao, F.; Wu, Y.; Yao, Y.; Sun, K.; Zhang, X.; Winowiecki, L.; Sun, Y. Predicting the climate change impacts on water-carbon coupling cycles for a loess hilly-gully watershed. *J. Hydrol.* **2020**, *581*, 124388. [CrossRef]
57. Rong, T.; Long, L.H. Quantitative Assessment of NPP Changes in the Yellow River Source Area from 2001 to 2017. In Proceedings of the IOP Conference Series: Earth and Environmental Science; IOP Publishing: Bristol, UK, 2021; p. 012002.
58. Pengfei, C. Monthly NPP dataset covering China′ s terrestrial ecosystems at North of 18 N (1985—2015). *J. Glob. Chang. Data Discov.* **2019**, *3*, 34–41.
59. Zheng, Y.; Dong, L.; Xia, Q.; Liang, C.Z.; Wang, L.X.; Shao, Y.P. Effects of revegetation on climate in the Mu Us Sandy Land of China. *Sci. Total Environ.* **2020**, *739*, 139958. [CrossRef]
60. Li, J.; Wang, Z.L.; Lai, C.G.; Wu, X.Q.; Zeng, Z.Y.; Chen, X.H.; Lian, Y.Q. Response of net primary production to land use and land cover change in mainland China since the late 1980s. *Sci. Total Environ.* **2018**, *639*, 237–247. [CrossRef]
61. Ge, W.; Deng, L.Q.; Wang, F.; Han, J.Q. Quantifying the contributions of human activities and climate change to vegetation net primary productivity dynamics in China from 2001 to 2016. *Sci. Total Environ.* **2021**, *773*, 145648. [CrossRef]
62. Kamali, A.; Khosravi, M.; Hamidianpour, M. Spatial-temporal analysis of net primary production (NPP) and its relationship with climatic factors in Iran. *Environ. Monit. Assess.* **2020**, *192*, 718. [CrossRef] [PubMed]
63. Jiang, K.; Pan, Z.; Pan, F.; Wang, J.; Han, G.; Song, Y.; Zhang, Z.; Huang, N.; Ma, S.; Chen, X. Influence patterns of soil moisture change on surface-air temperature difference under different climatic background. *Sci. Total Environ.* **2022**, *822*, 153607. [CrossRef] [PubMed]
64. Huang, N.Y.; Mondal, P.; Cook, B.I.; McDermid, S. Moisture and temperature influences on nonlinear vegetation trends in Serengeti National Park. *Environ. Res. Lett.* **2021**, *16*, 094049. [CrossRef]
65. Gao, Q.; Li, Y.; Wan, Y.; Qin, X.; Jiangcun, W.; Liu, Y. Dynamics of alpine grassland NPP and its response to climate change in Northern Tibet. *Clim. Chang.* **2009**, *97*, 515–528. [CrossRef]
66. Yan, Y.; Xu, X.; Liu, X.; Wen, Y.; Ou, J. Assessing the contributions of climate change and human activities to cropland productivity by means of remote sensing. *Int. J. Remote Sens.* **2020**, *41*, 2004–2021. [CrossRef]

Disclaimer/Publisher's Note: The statements, opinions and data contained in all publications are solely those of the individual author(s) and contributor(s) and not of MDPI and/or the editor(s). MDPI and/or the editor(s) disclaim responsibility for any injury to people or property resulting from any ideas, methods, instructions or products referred to in the content.